Multiorbital Interactions and Spin Polarization in Single Rare-Earth Adatoms

Massine Kelai,[1,2] Stefano Reale,[1,2,3] Roberto Robles,[4] Jaehyun Lee,[1,5] Divya Jyoti,[4,6] Philippe Ohresser,[7] Edwige Otero,[7] Fadi Choueikani,[7] Fabrice Scheurer,[8] Nicolás Lorente,[4,6] Deung-Jang Choi,[4,6,9] Aparajita Singha,[10] and Fabio Donati[1,5,*]

[1]*Center for Quantum Nanoscience (QNS), Institute for Basic Science (IBS), Seoul 03760, Republic of Korea*
[2]*Ewha Womans University, Seoul 03760, Republic of Korea*
[3]*Department of Energy, Politecnico di Milano, Milano 20133, Italy*
[4]*Centro de Física de Materiales CFM/MPC (CSIC-UPV/EHU), Donostia-San Sebastián, Spain*
[5]*Department of Physics, Ewha Womans University, Seoul 03760, Republic of Korea*
[6]*Donostia International Physics Center (DIPC), Donostia-San Sebastián, Spain*
[7]*Synchrotron SOLEIL, L'Orme des Merisiers, 91190 Saint-Aubin, France*
[8]*Institut de Physique et Chimie des Matériaux de Strasbourg, Strasbourg, France*
[9]*Ikerbasque, Basque Foundation for Science, 48013 Bilbao, Spain*
[10]*Max Planck Institute for Solid State Research, Stuttgart, Germany*

(Received 27 May 2024; revised 13 November 2024; accepted 11 July 2025; published 5 September 2025)

Surface-adsorbed rare-earth nanostructures are ideal platforms to investigate the interplay between intra-atomic interactions and multiorbital spin configurations. However, addressing these properties has posed severe experimental and theoretical challenges. Here, we use the orbital selectivity offered by x-ray absorption spectroscopy to quantify the Coulomb integrals of Nd atoms on conductive surfaces directly from experimental quantities, as well as the variation of individual orbital occupation upon cluster nucleation. Using x-ray magnetic circular dichroism we identify magnetic moments of the order of $0.1-0.2\ \mu_B$ at the $5d$ orbitals and their magnetic coupling with the $4f$ spins. Our results validate orbital-resolved x-ray spectroscopy as a reliable method for quantifying complex multiorbital interactions in surface-adsorbed lanthanides.

DOI: 10.1103/mkqz-p424

Rare-earth (RE) elements represent exquisite building blocks for materials exhibiting intriguing properties such as frustrated magnetism [1,2], superconductivity [3,4], heavy fermion [5], and mixed-valence behavior [6–10]. The interplay between localized $4f$ and itinerant $5d6s$ valence orbitals governs ultrafast spin dynamics [11–15], mediates complex magnetic interactions [12,14,16], and drives the formation of surface architectures [17–19]. It is also shapes the magnetic anisotropy and enhances spin relaxation of atomic and molecular magnets [20–26].

Individual RE atoms on surfaces with open $4f$ shells have been explored as model systems for ultra-high-density magnetic storage [27–31], spin qubits [32], and platforms for the emergence of exotic many-body states [33,34]. In these systems, the presence of unpaired $5d6s$ electrons significantly enhances the spin contrast in transport measurements [35,36] and the coupling with substrate electrons [37]. Despite theoretical efforts to resolve the multiorbital configuration of RE adatoms [31,35,37,38], orbital-resolved measurements have only been demonstrated for Gd and Ho atoms on MgO/Ag(100) [39] while remaining unexplored on conductive surfaces.

On surfaces, RE atoms show two distinct $4f$ occupations, namely atomiclike $4f^n$ and bulklike $4f^{n-1}$ [31,40–42]. The determining factors for the $4f$ occupation and spin configuration of the ground state are the Coulomb integrals and polarization of the outer $5d6s$ shells, which are shaped by coordination and RE-substrate hybridization [43–45]. However, accurately computing these quantities and predicting the many-body ground state of strongly correlated systems containing REs remain difficult [43,46–55]. Specifically, multiplet calculations show limitations when used for analyzing valence states in a metal environment [56,57] or upon cluster nucleation, as electron delocalization disrupts the atomic orbital character. This highlights the need for experimental methods to advance the understanding of multiorbital interactions in these systems.

We use orbital-resolved x-ray absorption spectroscopy (XAS) to analyze the multiorbital configuration of Nd adatoms. Nd exhibits an atomiclike $4f^4$ occupation on weakly interacting substrates [highly oriented pyrolytic

*Contact author: donati.fabio@qns.science

Published by the American Physical Society under the terms of the Creative Commons Attribution 4.0 International license. Further distribution of this work must maintain attribution to the author(s) and the published article's title, journal citation, and DOI.

graphite (HOPG), Ag(100), and graphene (Gr) on Cu(111)], shifting to a bulklike $4f^3$ state on strongly interacting substrates [Pb(111)] or upon cluster nucleation. Leveraging the surface sensitivity of the $M_{2,3,4,5}$ series [39], we identify substrate-dependent spectral variations that reveal changes in the orbital occupation and enable direct quantification of multiorbital Coulomb interactions from experiment. X-ray magnetic circular dichroism (XMCD) reveals spin polarization of Nd atoms and clusters with orbital sensitivity, along with their characteristic interorbital magnetic coupling. For the $5d$ orbitals, we find a magnetic moment of $0.1-0.2\ \mu_B$, consistent with density-functional theory (DFT). These results validate our approach for addressing the complexity of RE nanostructures on surfaces and provide a benchmark for theoretical models.

XAS and XMCD measurements were conducted on the DEIMOS beamline [58–60] at the SOLEIL synchrotron. We acquired the sum and difference of right and left circular polarization absorptions under a magnetic field $B = 6$ T and a temperature $T = 1.8$ K. To prevent surface diffusion, we sublimated minute amounts of Nd (less than 1% of a monolayer, ML) onto the sample kept below 10 K, while larger Nd coverages were employed to promote the statistical growth of clusters [61]. Surface and orbital sensitivity were achieved through soft x-ray absorption at specific M edges. The electric dipole selection rules impose a unitary change in the total orbital quantum number [62]. Consequently, the $M_{4,5}$ transitions create a hole in the $3d$ core levels by transferring one electron to $4f$, while the $M_{2,3}$ transitions promote one electron from the $3p$ to the $5d6s$ states, as illustrated in Fig. 1 [39]. As demonstrated further in this Letter, each transition provides complementary information to map the multiorbital configuration of RE atoms.

In line with a previous study [41], we expect the ground state of Nd on surfaces to be either atomiclike $4f^4$ or bulklike $4f^3$ depending on the atom-substrate interaction and coordination. As illustrated in Figs. 2(a)–2(c), on HOPG and on Ag(100), the M_5 XAS of isolated Nd atoms distinctly reflects a dominant $4f^4$ atomiclike configuration [42], while on Pb(111), the XAS maximum is observed at a higher energy, with an absorption line indicating a $4f^3$ bulklike configuration [63]. This difference in $4f$ occupation suggests a weaker adatom-substrate interaction on HOPG and Ag(100) compared to Pb(111) [41]. To understand the substrate dependence of $4f$ occupation, we compare our findings with DFT calculations performed using the generalized gradient approximation for the exchange-correlation functional and employing a plane-wave basis and projector augmented wave potentials [64]. For HOPG and Ag(100), we find that Nd atoms exhibit preferential adsorption at the hollow site and occupation of $4f^4$, while surface embedding on Pb(111) is preferred [64]. The increased coordination promotes a $4f^3$ configuration

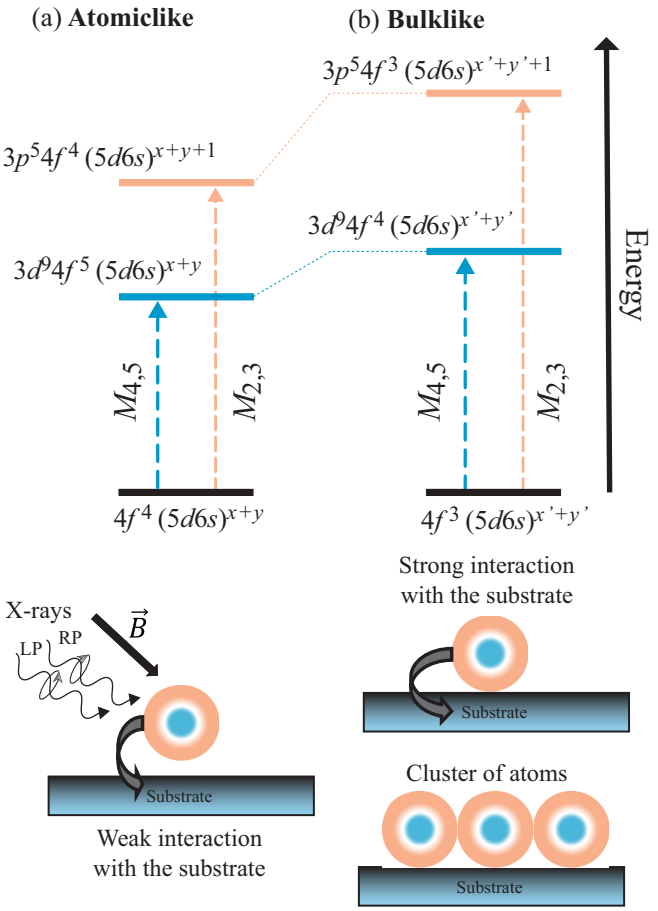


FIG. 1. XAS transition diagram for Nd in different configurations: (a) atomiclike configuration with weak substrate interaction (lower left sketch), and (b) bulklike configurations corresponding to either strong interaction with the substrate (lower middle sketch) or clustering (lower right sketch). $M_{4,5}$ (blue) and $M_{2,3}$ (salmon) probe the $4f$ and $5d6s$ occupancies, respectively. Energy differences denoted highlight transitions involving different electron arrangements in the $4f$ and $5d6s$ orbitals. x (resp. x') and y (resp. y') represent the number of electrons in the $5d$ and 6s orbitals in the atomic-like (resp. bulklike) ground state configuration. The magnetic field vector ($\vec{B}$) and the wave vector of circularly polarized photons are parallel.

and an opposite sign of the magnetic anisotropy on this substrate [29]. This also impacts the occupation of the $5d$ orbitals, as will be discussed further in the text.

By increasing the Nd coverage, the maximum of the M_5 XAS for both HOPG and Ag(100) shifts to higher energies and aligns with that observed for Pb(111), indicating a transition from a $4f^4$ to a $4f^3$ configuration following the formation of dimers and larger clusters [42]. A similar trend is observed for Nd on Gr/Cu(111) [64]. In contrast, on Pb(111), the spectrum shows a negligible redshift upon cluster nucleation ($\Delta_5 = -0.1$ eV), suggesting no significant changes in the $4f$ occupation. The scenario becomes more diversified for the spectra acquired at the M_3 edge, as presented in Figs. 2(d)–2(f), and is similarly visible at the

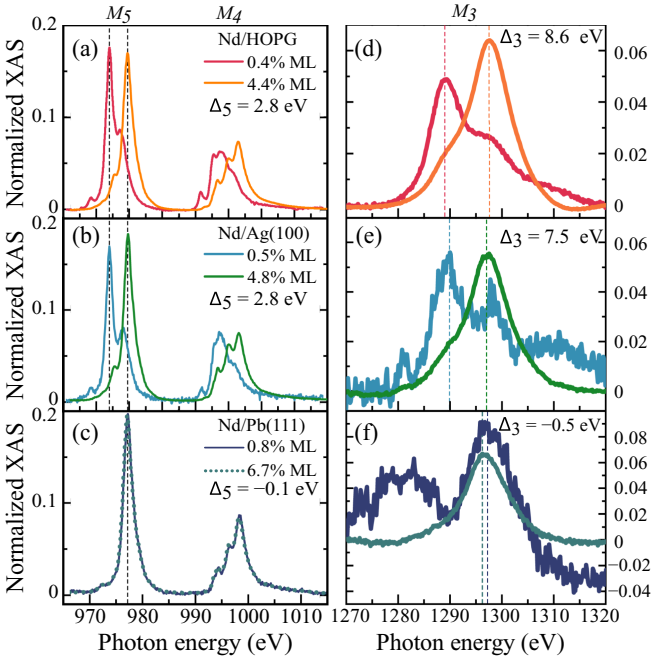


FIG. 2. X-ray absorption of Nd on HOPG, Ag(100), and Pb(111) at the $M_{4,5}$ edge [(a), (b), (c)] and M_3 edge [(d), (e), (f)]. Dashed lines mark the XAS maxima for each sample. The energy differences between the atoms' and clusters' XAS maxima at the M_5 and M_3 edges are marked as Δ_5 and Δ_3, respectively. In Fig. 2(f), the bump at 1280 eV (dark blue trace) is due to substrate background absorption, which could not be accurately subtracted because of a limited signal-to-noise ratio. The Nd coverage in % ML is indicated in the legend. The measurements have been acquired at 6 T and 1.8 K along the easy magnetization axis for isolated Nd atoms on each substrate: normal incidence on HOPG and Ag(100), and grazing incidence (60° off-normal) on Pb(111) [64].

M_2 edge [64]. Again on HOPG and Ag(100), the XAS maximum of the ensemble of isolated atoms moves to higher energy upon cluster nucleation. In this case the energy difference is larger than that observed for the M_5 edge and displays variations between the two substrates, i.e. $\Delta_3 = 8.6$ eV and 7.5 eV for HOPG and Ag(100), respectively. Conversely, Nd on Pb(111) exhibits a much smaller and opposite shift of the XAS maximum ($\Delta_3 = -0.5$ eV). These findings lead us to conclude that on both M_5 and M_3 edges the position of the XAS maxima is mostly determined by the $4f$ occupation. However, the larger energy differences observed at the M_3 edge allow detecting sizable substrate-dependent shifts, which offers the possibility of quantifying changes in the electronic configuration of the outer shells.

Differently from RE atoms on oxide layers [39], the interaction with conductive surfaces causes the $5d6s$ orbitals of RE atoms and clusters to become dispersive, which renders multiplet calculations unreliable for determining the electronic configuration. To overcome this issue, we developed a multiorbital analytical model to compute the charge variations and Coulomb integrals from the quantities Δ_5 and Δ_3. In its simplest formulation, the model includes only $4f$ and $5d$ orbitals, although it can be generalized to an arbitrary set of orbitals and XAS transition [64]. Specific to Nd, the relatively symmetric multiplet structure enables estimating the $\Delta_{5,3}$ from the energy difference between the maxima at the $M_{5,3}$ edges, respectively, although the peak barycenter can alternatively be used [64]. In the two-orbital model, the energy difference of Δ_5 and Δ_3 can be expressed as

$$\Delta_5 = \delta q_{4f}(U_{4f4f} - U_{3d4f}) + \delta q_{5d}(U_{4f5d} - U_{3d5d}), \quad (1)$$

$$\Delta_3 = \delta q_{4f}(U_{4f5d} - U_{3p4f}) + \delta q_{5d}(U_{5d5d} - U_{3p5d}), \quad (2)$$

where $\delta q_{4f,5d}$ refers to the difference between the cluster and atom occupations at the $4f$ and $5d$ orbitals, respectively, and $U_{\alpha,\beta}$ are the intra- and intershell Coulomb integrals. Although Eqs. (1) and (2) are exact for integer charge variations, the linear response of the interaction energy with the orbital occupation ensures their validity also with fractional charges [80]. In both equations, the terms are arranged in increasing values of the Coulomb integrals. All terms contain a difference between the multiorbital Coulomb integrals involving core states and another one involving only $4f$ or $5d$ states. To quantify the changes in orbital occupation, we fit the values of Δ_5 and Δ_3 using Eqs. (1) and (2) through a Bayesian optimization procedure [64,81]. To account for the electron-electron screening from the substrate, the Coulomb integrals are computed as $U_{\alpha,\beta} = \sqrt{\kappa_\alpha \kappa_\beta} F^0_{\alpha,\beta}$, where $\kappa_{\alpha,\beta}$ are effective screening coefficients and $F^0_{\alpha,\beta}$ are the first-order Slater integrals obtained from a Hartree-Fock atomic calculation [82]. To avoid overparametrization, we assume $\kappa_{3p} = \kappa_{3d} = \kappa_{4f}$, as these orbitals are not significantly hybridized with the substrate, while we take κ_{5d} as an independent value. In addition, we fix the value of δq_{4f} from the energy shift of the M_5 edge and we obtain δq_{5d} from the fit (one for each substrate), under the assumption of a cluster-size independent charge transfer. We constrain the fit by imposing charge conservation upon cluster nucleation, i.e., $\delta q_{4f} + \delta q_{5d} + \delta q_{env} = 0$, where the environment charge variation (δq_{env}) describes the charge transfer toward the $6s$ orbitals, as well as to the substrate. We constrain the latter term between two extreme cases, namely, $-0.5 \leq \delta q_{env} \leq -\delta q_{4f}$. The lower bound represents the maximum back donation from the environment, quantified from typically observed charge variation in RE [39,40] and alkaline adatoms [83] upon cluster nucleation. The upper bound corresponds to the case where all the $4f$ charge is transferred toward the environment without altering the $5d$ occupation.

As shown in Table I, the fitted charge variations exhibit a clear substrate dependence, with a smaller increase in the

TABLE I. Charge variation for Nd upon cluster nucleation on different substrates, obtained from the fit to the data using Eqs. (1) and (2). The fit results are obtained for $\kappa_{3p,3d,4f} = 0.290 \pm 0.003$ and $\kappa_{5d} = 0.054 \pm 0.006$.

Nd on	HOPG	Gr/Cu(111)	Ag(100)	Pb(111)
δq_{4f}	−1	−1	−1	0
δq_{5d}	0.57 (9)	0.30 (9)	1.30 (10)	0.47 (3)

$5d$ occupation on carbon surfaces. In these systems, most rare earths attain an atomiclike $4f^n$ configuration with an open $6s$ shell [35,36,42] due to charge transfer to the substrate [84]. Upon cluster formation, two effects increase the occupation of the $5d6s$ orbitals: (1) the $4f^n$ occupation decreases by one, promoting an electron to the valence shell for bonding [42], and (2) the charge transfer per atom reduces [83], localizing more charge on valence orbitals. On HOPG and Gr/Cu(111), Nd nucleation only produces a marginal $5d$ charge increase, implying that most charge is transferred to the open $6s$ orbitals (also confirmed with the three-orbital model [64]). Conversely, on Ag(100) and Pb(111), $5d$ orbitals gather more charge than what is transferred from the $4f$, indicating essentially closed $6s$ shells, with charge instead accumulating in $5d$ orbitals via $4f$ promotion and substrate backdonation. Our Coulomb integral values $U_{4f4f} = 7.9$ eV and $U_{4f5d} = 1.5$ eV closely resemble those from bulk Nd [47,85,86] and various lanthanum compounds [87], respectively. Applying our method to other surface-RE systems [41] yields values consistent with previous reports for bulk compounds [64,85,86], validating its reliability in estimating multi-orbital Coulomb interactions and charge variations in RE adatoms.

Through XMCD we probe the orbital-resolved spin polarization of RE atoms and its variation occurring upon nucleation. Figure 3(a) shows the XMCD of Nd atoms and clusters at the $M_{4,5}$ edges on Ag (100) revealing the magnetism of $4f$ electrons. Among all samples, Nd on Ag (100) show the largest XMCD, which is maximal at normal incidence, indicating an out-of-plane easy axis [64]. As expected for early lanthanides, the largest dichroism is found at the M_4 edge [42,88]. Upon clustering, the XMCD peak shifts to higher energy by the same amount found for the XAS, and its intensity decreases.

Sum rules [89,90] give an estimate of the magnetic moments, which are accurate for Nd coverages $< 1\%$, as the ensemble is essentially composed of single atoms. At higher coverages, cluster nucleation progressively introduces different species [91], whose contribution cannot be easily deconvolved. Moreover, full magnetic saturation is only attained for single Nd adatoms on Ag (100), limiting the quantitative analysis of higher Nd coverages. We therefore focus on comparing the overall sum rule trends to identify the sign of the coupling among magnetic moments. As shown in Figs. 3(b) and 3(c), on all substrates

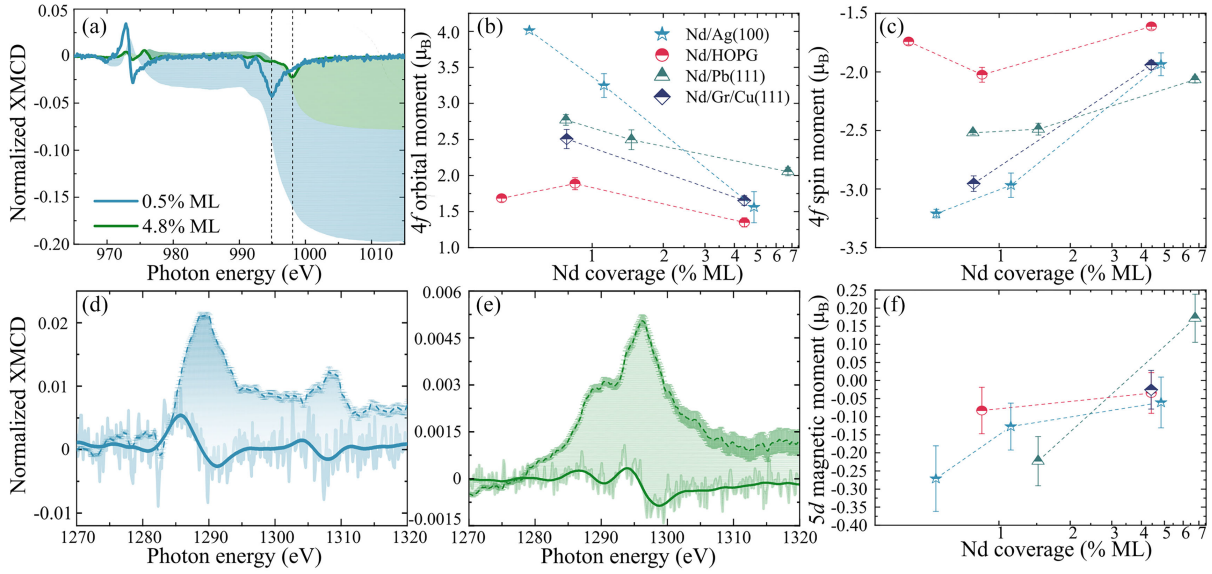


FIG. 3. Normalized and integrated XMCD spectra at the $M_{4,5}$ edges for Nd on Ag (100) are presented for the lowest (in blue) and highest (in cyan) coverages (a). Dashed vertical lines denote the energy corresponding to the XMCD maximum for both configurations. $4f$ orbital and spin moments, obtained through sum rules, are shown in (b) and (c). Normalized and integrated XMCD spectra at the M_3 edge for individual atoms and clusters are depicted in (d) and (e), respectively. Estimated magnetic moments are highlighted in panel (f). The difference in the number of points between (b), (c) and (f) is due to the lack of reliable M_3 XMCD at coverages below 1% ML due to very low signal-to-noise ratio. Raw data, displayed in transparent lines, are smoothed using a Sawatzky-Golay method (full lines) for enhanced clarity. The error bar is represented by the deviation around the central line of the XMCD integral (dashed lines). For each substrate, data were acquired at 6 T and 1.8 K along the easy magnetization axis of isolated Nd atoms [64].

except HOPG, we find the largest magnetic moments for the lowest coverage of Nd, with spin (μ_S^{4f}) and orbital (μ_L^{4f}) moments in opposite alignment, as expected for an early lanthanide. The decrease in magnetic moment with increasing coverage does not correlate with the change expected for a free atom, as the total magnetic moment is lower for $4f^4$ than $4f^3$. This either suggests a reorientation of the easy axis [29] or the formation of noncollinear magnetic states [92,93], both preventing saturation at the maximum available field (6 T) [64].

The XMCD at the M_3 edge [Figs. 3(d) and 3(e)] exhibits a characteristic peak-derivative shape for Nd atoms and clusters on Ag (100), as well as on all other substrates [64]. This peak-derivative reverses sign at the M_2 edge [64], as previously observed for Gd on MgO/Ag (100) [39]. Comparison with multiplet calculations indicates that the XMCD signal is largely dominated by transitions to the $5d$ states, even in systems with an open $6s$ shell—possibly due to stronger renormalization of the $6s$ Slater integrals [64]. Notably, the XMCD shape for Nd is opposite in sign to that of Gd [39]. This reflects the fact that in Gd, both the $4f$ and $5d$ spins align with the external field due to its vanishing orbital moment. In contrast, for Nd, the dominant $4f$ orbital moment aligns with the field, while spin-orbit coupling causes the $4f$ spin to align antiparallel. Through exchange coupling, the $5d$ spin also aligns opposite to the field, resulting in reversed $M_{2,3}$ XMCD.

Within the same limitations discussed for the $4f$ electrons, we follow the trend of the $5d$ magnetic moments by applying sum rules to the $M_{2,3}$ XMCD. As shown in Figs. 3(d) and 3(e), a positive M_3 XMCD integral is observed for atoms and clusters on Ag (100), as well as for all samples, while the lower intensity of the M_2 XMCD often leads to large uncertainties [64]. These uncertainties can be reduced by computing the total $5d$ magnetic moment μ_{5d} [64], summarized in Fig. 3(f). Notably, μ_{5d} has the same sign as μ_S^{4f} and follows a similar coverage trend [Fig. 3(c)], confirming the parallel $4f$-$5d$ spin coupling. Although smaller in magnitude than $\mu_{S,L}^{4f}$, μ_{5d} values are consistent with those reported for ferromagnetic RE bulk compounds [94]. As shown in Table II, the sum-rule estimates are close to DFT values. The small discrepancies likely reflect DFT's well-known limitations in treating exchange and correlation in strongly correlated systems. For Nd on Ag (100) and HOPG, the low polarization arises from the small $5d$ occupation, while for Pb (111), it is due to the strong overlap between spin-split $5d$ states [64].

TABLE II. Magnetic moments (μ_{5d}) and occupation (q_{5d}) of the $5d$ orbitals of Nd. Magnetic moments are given in Bohr magnetons μ_B.

	XMCD		DFT	
Coverage (ML)	0.4%	0.8% − 1.6%	Single atom	
Nd on	$\lvert\mu_{5d}\rvert$	$\lvert\mu_{5d}\rvert$	μ_{5d}	q_{5d}
HOPG	—	0.08 (6)	0.09	0.24
Ag(100)	0.27.(9)	0.13 (7)	0.06	0.27
Pb(111)	—	0.22 (7)	0.17	0.83

Our approach, based on orbital-resolved absorption spectroscopy, offers a framework to quantify multiorbital Coulomb interactions among isolated surface atoms and track charge-state changes during cluster nucleation and, possibly, on-surface reactions [17–19]. Its main strength lies in determining these quantities from the XAS peak energy, without relying on multiplet theory, and providing an experimental basis for theoretical models of strongly correlated atoms. By probing spin polarization in the $4f$ and $5d$ orbitals, our method complements scanning probe techniques, which are more sensitive to spatially extended $6s$ states [35,36], enabling a more complete characterization of surface RE magnetism and multi-open-shell systems.

Acknowledgments—Experiments were performed on the DEIMOS beamline at SOLEIL Synchrotron, France (Proposals No. 20191894 and No. 20220066). We are grateful to the SOLEIL staff for smoothly running the facility. The authors would like to thank Bernard Muller for his significant contribution to the construction of DEIMOS beamline (design and engineering) and Florian Leduc for his support. The MBE chamber used during the XAS/XCMD experiment on DEIMOS has been funded by the Agence National de la Recherche; Grant ANR-05-NANO-073. M. K., S. R., J. L., and F. D. acknowledge support from the Institute for Basic Science under Grant IBS-R027-D1. D.-J. C., R. R. and N. L. thank projects PID2021-127917NB-I00 by MCIN/AEI/10.13039/501100011033, 202260I187 by CSIC, QUAN000021-01 by Gipuzkoa Provincial Council, and PIBA-2024-1-0008 and IT-1527-22 by Basque Government.

[1] J. E. Greedan, J. Alloys Compd. **408–412**, 444 (2006).
[2] J. Lago, I. Živković, B. Z. Malkin, J. Rodriguez Fernandez, P. Ghigna, P. Dalmas de Rêotier, A. Yaouanc, and T. Rojo, Phys. Rev. Lett. **104**, 247203 (2010).
[3] L. Sun, X. Dai, C. Zhang, W. Yi, G. Chen, N. Wang, L. Zheng, Z. Jiang, X. Wei, Y. Huang, J. Yang, Z. Ren, W. Lu, X. Dong, G. Che, Q. Wu, H. Ding, J. Liu, T. Hu, and Z. Zhao, Europhys. Lett. **91**, 57008 (2010).
[4] H. Yamaoka, Y. Ikeda, I. Jarrige, N. Tsujii, Y. Zekko, Y. Yamamoto, J. Mizuki, J.-F. Lin, N. Hiraoka, H. Ishii, K.-D. Tsuei, T. Kobayashi, F. Honda, and Y. Ōnuki, Phys. Rev. Lett. **113**, 086403 (2014).
[5] J.-P. Rueff, S. Raymond, M. Taguchi, M. Sikora, J.-P. Itié, F. Baudelet, D. Braithwaite, G. Knebel, and D. Jaccard, Phys. Rev. Lett. **106**, 186405 (2011).
[6] B. Batlogg, Phys. Rev. B **23**, 650 (1981).
[7] T. Matsumura, T. Kosaka, J. Tang, T. Matsumoto, H. Takahashi, N. Môri, and T. Suzuki, Phys. Rev. Lett. **78**, 1138 (1997).

[8] C. Grazioli, Z. Hu, M. Knupfer, G. Graw, G. Behr, M. S. Golden, J. Fink, H. Giefers, G. Wortmann, and K. Attenkofer, Phys. Rev. B **63**, 115107 (2001).

[9] N. P. Butch, J. Paglione, P. Chow, Y. Xiao, C. A. Marianetti, C. H. Booth, and J. R. Jeffries, Phys. Rev. Lett. **116**, 156401 (2016).

[10] B. Joseph, R. Torchio, C. Benndorf, T. Irifune, T. Shinmei, R. Pöttgen, and A. Zerr, Phys. Chem. Chem. Phys. **19**, 17526 (2017).

[11] M. Wietstruk, A. Melnikov, C. Stamm, T. Kachel, N. Pontius, M. Sultan, C. Gahl, M. Weinelt, H. A. Dürr, and U. Bovensiepen, Phys. Rev. Lett. **106**, 127401 (2011).

[12] I. Radu, K. Vahaplar, C. Stamm, T. Kachel, N. Pontius, H. A. Dürr, T. A. Ostler, J. Barker, R. F. L. Evans, R. W. Chantrell, A. Tsukamoto, A. Itoh, A. Kirilyuk, T. Rasing, and A. V. Kimel, Nature (London) **472**, 205 (2011).

[13] A. R. Khorsand, M. Savoini, A. Kirilyuk, A. V. Kimel, A. Tsukamoto, A. Itoh, and T. Rasing, Phys. Rev. Lett. **110**, 107205 (2013).

[14] N. Bergeard, V. López-Flores, V. Halté, M. Hehn, C. Stamm, N. Pontius, E. Beaurepaire, and C. Boeglin, Nat. Commun. **5**, 3466 (2014).

[15] B. Frietsch, J. Bowlan, R. Carley, M. Teichmann, S. Wienholdt, D. Hinzke, U. Nowak, K. Carva, P. M. Oppeneer, and M. Weinelt, Nat. Commun. **6**, 8262 (2015).

[16] L. Peters, S. Ghosh, B. Sanyal, C. Van Dijk, J. Bowlan, W. De Heer, A. Delin, I. Di Marco, O. Eriksson, M. I. Katsnelson, B. Johansson, and A. Kirilyuk, Sci. Rep. **6**, 19676 (2016).

[17] J. I. Urgel, B. Cirera, Y. Wang, W. Auwärter, R. Otero, J. M. Gallego, M. Alcamí, S. Klyatskaya, M. Ruben, F. Martín, R. Miranda, D. Ecija, and J. V. Barth, Small **11**, 6358 (2015).

[18] J. I. Urgel, D. Écija, G. Lyu, R. Zhang, C.-A. Palma, W. Auwärter, N. Lin, and J. V. Barth, Nat. Chem. **8**, 657 (2016).

[19] D. Écija, J. I. Urgel, A. P. Seitsonen, W. Auwërter, and J. V. Barth, Acc. Chem. Res. **51**, 365 (2018).

[20] F. Luis, A. Repollés, M. J. Martínez-Pérez, D. Aguilá, O. Roubeau, D. Zueco, P. J. Alonso, M. Evangelisti, A. Camón, J. Sesé, L. A. Barrios, and G. Aromí, Phys. Rev. Lett. **107**, 117203 (2011).

[21] D. Aguilá, L. A. Barrios, V. Velasco, O. Roubeau, A. Repollés, P. J. Alonso, J. Sesé, S. J. Teat, F. Luis, and G. Aromí, J. Am. Chem. Soc. **136**, 14215 (2014).

[22] K. R. Meihaus, M. E. Fieser, J. F. Corbey, W. J. Evans, and J. R. Long, J. Am. Chem. Soc. **137**, 9855 (2015).

[23] F. Liu, D. S. Krylov, L. Spree, S. M. Avdoshenko, N. A. Samoylova, M. Rosenkranz, A. Kostanyan, T. Greber, A. U. B. Wolter, B. Büchner, and A. A. Popov, Nat. Commun. **8**, 16098 (2017).

[24] C. A. Gould, K. R. McClain, J. M. Yu, T. J. Groshens, F. Furche, B. G. Harvey, and J. R. Long, J. Am. Chem. Soc. **141**, 12967 (2019).

[25] V. Dubrovin, A. A. Popov, and S. Avdoshenko, Chem. Commun. **55**, 13963 (2019).

[26] V. Dubrovin, A. A. Popov, and S. M. Avdoshenko, Inorg. Chem. Front. **8**, 2373 (2021).

[27] R. Baltic, M. Pivetta, F. Donati, C. Wäckerlin, A. Singha, J. Dreiser, S. Rusponi, and H. Brune, Nano Lett. **16**, 7610 (2016).

[28] F. Donati, S. Rusponi, S. Stepanow, C. Wäckerlin, A. Singha, L. Persichetti, R. Baltic, K. Diller, F. Patthey, E. Fernandes, J. Dreiser, Z. Sljivancanin, K. Kummer, C. Nistor, P. Gambardella, and H. Brune, Science **352**, 318 (2016).

[29] A. Singha, F. Donati, C. Wäckerlin, R. Baltic, J. Dreiser, M. Pivetta, S. Rusponi, and H. Brune, Nano Lett. **16**, 3475 (2016).

[30] F. D. Natterer, K. Yang, W. Paul, P. Willke, T. Choi, T. Greber, A. J. Heinrich, and C. P. Lutz, Nature (London) **543**, 226 (2017).

[31] F. Donati, M. Pivetta, C. Wolf, A. Singha, C. Wäckerlin, R. Baltic, E. Fernandes, J.-G. de Groot, S. L. Ahmed, L. Persichetti, C. Nistor, J. Dreiser, A. Barla, P. Gambardella, H. Brune, and S. Rusponi, Nano Lett. **21**, 8266 (2021).

[32] S. Reale, A. Singha, S. L. Ahmed, D. Krylov, L. Colazzo, C. Wolf, C. S. Casari, A. Barla, E. Fernandes, F. Patthey, M. Pivetta, S. Rusponi, H. Brune, and F. Donati, Phys. Rev. B **107**, 045427 (2023).

[33] A. Yazdani, B. A. Jones, C. P. Lutz, M. F. Crommie, and D. M. Eigler, Science **275**, 1767 (1997).

[34] H. Ding, Y. Hu, M. T. Randeria, S. Hoffman, O. Deb, J. Klinovaja, D. Loss, and A. Yazdani, Proc. Natl. Acad. Sci. U.S.A. **118**, e2024837118 (2021).

[35] M. Pivetta, F. Patthey, I. Di Marco, A. Subramonian, O. Eriksson, S. Rusponi, and H. Brune, Phys. Rev. X **10**, 031054 (2020).

[36] A. Curcella, D. Sblendorio, S. Rusponi, M. Pivetta, F. Patthey, and H. Brune, Phys. Rev. Lett. **130**, 106702 (2023).

[37] D. Coffey, J. L. Diez-Ferrer, D. Serrate, M. Ciria, C. d. l. Fuente, and J. I. Arnaudas, Sci. Rep. **5**, 13709 (2015).

[38] A. L. Kozub, A. B. Shick, F. Máca, J. Kolorenč, and A. I. Lichtenstein, Phys. Rev. B **94**, 125113 (2016).

[39] A. Singha, D. Sostina, C. Wolf, S. L. Ahmed, D. Krylov, L. Colazzo, P. Gargiani, S. Agrestini, W.-S. Noh, J.-H. Park, M. Pivetta, S. Rusponi, H. Brune, A. J. Heinrich, A. Barla, and F. Donati, ACS Nano **15**, 16162 (2021).

[40] C. Nistor, A. Mugarza, S. Stepanow, P. Gambardella, K. Kummer, J. L. Diez-Ferrer, D. Coffey, C. de la Fuente, M. Ciria, and J. I. Arnaudas, Phys. Rev. B **90**, 064423 (2014).

[41] A. Singha, R. Baltic, F. Donati, C. Wäckerlin, J. Dreiser, L. Persichetti, S. Stepanow, P. Gambardella, S. Rusponi, and H. Brune, Phys. Rev. B **96**, 224418 (2017).

[42] R. Baltic, F. Donati, A. Singha, C. Wäckerlin, J. Dreiser, B. Delley, M. Pivetta, S. Rusponi, and H. Brune, Phys. Rev. B **98**, 024412 (2018).

[43] A. Kotani, T. Jo, and J. Parlebas, Adv. Phys. **37**, 37 (1988).

[44] A. Bianconi, M. Campagna, and S. Stizza, Phys. Rev. B **25**, 2477 (1982).

[45] F. Baudelet, C. Giorgetti, S. Pizzini, C. Brouder, E. Dartyge, A. Fontaine, and J. P. Kappler, J. Electron Spectrosc. Relat. Phenom. **62**, 153 (1993).

[46] O. Gunnarsson and K. Schönhammer, Phys. Rev. B **28**, 4315 (1983).

[47] D. Van Der Marel and G. A. Sawatzky, Phys. Rev. B **37**, 10674 (1988).

[48] D. Malterre, Phys. Rev. B **43**, 1391 (1991).

[49] J. M. Tomczak, Spectral and optical properties of correlated materials, Ph.D. thesis, Ecole Polytechnique, France, 2010.

[50] L. Vaugier, Electronic structure of correlated materials from first principles: Hubbard interaction and Hund's exchange, Ph.D. thesis, Ecole Polytechnique, France, 2011.

[51] H. Jiang, P. Rinke, and M. Scheffler, Phys. Rev. B **86**, 125115 (2012).

[52] J. M. Tomczak, L. V. Pourovskii, L. Vaugier, A. Georges, and S. Biermann, Proc. Natl. Acad. Sci. U.S.A. **110**, 904 (2013).

[53] B. Amadon, T. Applencourt, and F. Bruneval, Phys. Rev. B **89**, 125110 (2014).

[54] N. Lanatà, Y. Yao, C.-Z. Wang, K.-M. Ho, and G. Kotliar, Phys. Rev. X **5**, 011008 (2015).

[55] B.-L. Liu, Y.-C. Wang, Y. Liu, Y.-J. Xu, X. Chen, H.-Z. Song, Y. Bi, H.-F. Liu, and H.-F. Song, J. Chem. Phys. **158**, 084108 (2023).

[56] M. van Veenendaal, J. B. Goedkoop, and B. T. Thole, Phys. Rev. Lett. **78**, 1162 (1997).

[57] J. Parlebas, K. Asakura, A. Fujiwara, I. Harada, and A. Kotani, Phys. Rep. **431**, 1 (2006).

[58] P. Ohresser, E. Otero, F. Choueikani, K. Chen, S. Stanescu, F. Deschamps, T. Moreno, F. Polack, B. Lagarde, J.-P. Daguerre, F. Marteau, F. Scheurer, L. Joly, J.-P. Kappler, B. Muller, O. Bunau, and P. Sainctavit, Rev. Sci. Instrum. **85**, 013106 (2014).

[59] L. Joly, E. Otero, F. Choueikani, F. Marteau, L. Chapuis, and P. Ohresser, J. Synchrotron Radiat. **21**, 502 (2014).

[60] L. Joly, B. Muller, E. Sternitzky, J.-G. Faullumel, A. Boulard, E. Otero, F. Choueikani, J.-P. Kappler, M. Studniarek, M. Bowen, and P. Ohresser, J. Synchrotron Radiat. **23**, 652 (2016).

[61] H. Brune, Surf. Sci. Rep. **31**, 121 (1998).

[62] F. d. Groot and A. Kotani, *Core Level Spectroscopy of Solids*, Advances in Condensed Matter Science (CRC Press, Boca Raton, 2008).

[63] B. T. Thole, G. van der Laan, J. C. Fuggle, G. A. Sawatzky, R. C. Karnatak, and J.-M. Esteva, Phys. Rev. B **32**, 5107 (1985).

[64] See Supplemental Material at http://link.aps.org/supplemental/10.1103/mkqz-p424, which includes Refs. [65–79], for details on the theoretical model describing x-ray absorption energy shifts induced by configurational changes, including insights into the Bayesian optimization of charge transfer and Coulomb interaction parameters. It also provides additional XAS and XMCD data along with information on sample preparation, calibration procedures, sum-rule analysis, multiplet calculations, and density-functional theory.

[65] J. Lee, C. Urdaniz, S. Reale, K. Noh, D. Krylov, A. Doll, L. Colazzo, Y. Bae, C. Wolf, and F. Donati, Phys. Rev. B **109**, 235427 (2024).

[66] M. W. Haverkort, M. Zwierzycki, and O. K. Andersen, Phys. Rev. B **85**, 165113 (2012).

[67] B. Henke, E. Gullikson, and J. Davis, At. Data Nucl. Data Tables **54**, 181 (1993).

[68] B. N. Harmon and A. J. Freeman, Phys. Rev. B **10**, 1979 (1974).

[69] K. Fukui, H. Ogasawara, A. Kotani, I. Harada, H. Maruyama, N. Kawamura, K. Kobayashi, J. Chaboy, and A. Marcelli, Phys. Rev. B **64**, 104405 (2001).

[70] J. B. Goedkoop, A. Rogalev, M. Rogaleva, C. Neumann, J. Goulon, M. Van Veenendaal, and B. T. Thole, J. Phys. IV France **7**, C2 (1997).

[71] G. Kresse and J. Furthmüller, Comput. Mater. Sci. **6**, 15 (1996).

[72] G. Kresse and D. Joubert, Phys. Rev. B **59**, 1758 (1999).

[73] J. P. Perdew, K. Burke, and M. Ernzerhof, Phys. Rev. Lett. **77**, 3865 (1996).

[74] S. Grimme, J. Antony, S. Ehrlich, and H. Krieg, J. Chem. Phys. **132**, 154104 (2010).

[75] S. Grimme, S. Ehrlich, and L. Goerigk, J. Comput. Chem. **32**, 1456 (2011).

[76] S. L. Dudarev, G. A. Botton, S. Y. Savrasov, C. J. Humphreys, and A. P. Sutton, Phys. Rev. B **57**, 1505 (1998).

[77] F. Ma, Z. Zhang, D. Jiang, Z. Zhang, H. Kou, A. Strzep, Q. Tang, H. Zhou, M. Zhang, P. Zhang, S. Zhu, H. Yin, Q. Lv, Z. Li, Z. Chen, and L. Su, Cryst. Growth Des. **22**, 4480 (2022).

[78] D.-J. Choi, C. Rubio-Verdú, J. de Bruijckere, M. M. Ugeda, N. Lorente, and J. I. Pascual, Nat. Commun. **8**, 15175 (2017).

[79] C. Mier, A. Fétida, R. Robles, P. Boronat, D. Jyoti, N. Lorente, L. Limot, and D.-J. Choi, arXiv:2402.00644.

[80] M. Cococcioni and S. de Gironcoli, Phys. Rev. B **71**, 035105 (2005).

[81] P. I. Fraizer, arXiv:1807.02811.

[82] R. D. Cowan, *The Theory of Atomic Structure and Spectra*, 7th ed., Los Alamos Series in Basic and Applied Sciences (University of California Press, Berkeley, 1981).

[83] S. Kovarik, R. Robles, R. Schlitz, T. S. Seifert, N. Lorente, P. Gambardella, and S. Stepanow, Nano Lett. **22**, 4176 (2022).

[84] M. Pivetta, S. Rusponi, and H. Brune, Phys. Rev. B **98**, 115417 (2018).

[85] J. K. Lang, Y. Baer, and P. A. Cox, J. Phys. F **11**, 121 (1981).

[86] P. A. Cox, J. K. Lang, and Y. Baer, J. Phys. F **11**, 113 (1981).

[87] A. Kotani, M. Okada, T. Jo, A. Bianconi, A. Marcelli, and J. C. Parlebas, J. Phys. Soc. Jpn. **56**, 798 (1987).

[88] J. P. Schillé, F. Bertran, M. Finazzi, C. Brouder, J. P. Kappler, and G. Krill, Phys. Rev. B **50**, 2985 (1994).

[89] B. T. Thole, P. Carra, F. Sette, and G. Van Der Laan, Phys. Rev. Lett. **68**, 1943 (1992).

[90] P. Carra, B. T. Thole, M. Altarelli, and X. Wang, Phys. Rev. Lett. **70**, 694 (1993).

[91] C. Mocuta, P. Ohresser, and A. Barbier, Mater. Dev. **5**, 511 (2021).

[92] D. Gerion, A. Hirt, and A. Châtelain, Phys. Rev. Lett. **83**, 532 (1999).

[93] C. Van Dijk, J. Bowlan, W. A. De Heer, T. Rasing, and A. Kirilyuk, J. Phys. Chem. C **119**, 11153 (2015).

[94] T. Jo and S. Imada, J. Phys. Soc. Jpn. **62**, 3721 (1993).